Ferroelectrics, 485: 42–52, 2015

ISSN: 0015-0193 print / 1563-5112 online
DOI: 10.1080/00150193.2015.1060102

Taylor & Francis
Taylor & Francis Group

Local Structure Studies of Ti for $SrTi^{16}O_3$ and $SrTi^{18}O_3$ by Advanced X-ray Absorption Spectroscopy Data Analysis

A. ANSPOKS,[1,*] J. TIMOSHENKO,[1] D. BOCHAROV,[1]
J. PURANS,[1] F. ROCCA,[2] A. SARAKOVSKIS,[1]
V. TREPAKOV,[3,4] A. DEJNEKA,[4] AND M. ITOH[5]

[1]Institute of Solid State Physics, University of Latvia, Riga, LV-1063, Latvia
[2]IFN-CNR, Institute for Photonics and Nanotechnologies, Unit 'FBK-Photonics' of Trento, Povo (Trento), Italy
[3]Ioffe Physical-Technical Institute RAS, St-Petersburg, Russia
[4]Institute of Physics, AS CR, Prague, Czech Republic
[5]Tokyo Institute of Technology, Japan

Strontium titanate is a model quantum paraelectric in which in the region of dominating quantum statistics the ferroelectric instability is inhibited due to nearly complete compensation of the harmonic contribution into ferroelectric soft mode frequency by the zero-point motion contribution. The enhancement of atomic masses by the substitution of ^{18}O for ^{16}O decreases the zero-point atomic motion and low-T ferroelectricity in $SrTi^{18}O_3$ is realized. In this study we report on the local structure of Ti in $SrTi^{16}O_3$ and $SrTi^{18}O_3$ by Ti K-edge extended x-ray absorption fine structure measurements in temperature range 6 – 300 K.

Keywords Strontium titanate; quantum paraelectric; isotopic effect; X-ray absorption spectroscopy; local atomic structure; phase transitions

Introduction

Strontium titanate ($SrTiO_3$, STO) is a well-known and thoroughly studied model that is representative of the family of ABO_3 oxides and related materials [1]. At room temperature it has the cubic $O^1{}_h$ perovskite-type structure. Upon cooling STO undergoes a second order *Pm3m* ($O^1{}_h$) to *I4/mcm* ($D^{18}{}_{4h}$) antiferrodistorsive (AFD) phase transition (PT) T_C = 105 K with condensation of the R_{25} phonon mode at the Brillouin zone boundary [2, 3]. Following the Barrett formula [4, 5] the dielectric permittivity at first rises strongly upon cooling due to softening of the lowest TO_1 phonon mode (incipient ferroelectricity). At low temperatures, where the quantum statistics dominates the rising of dielectric permittivity saturates and the ferroelectric ordering is suppressed by quantum effects. The paraelectric phase of STO is retained down to the lowest temperatures (quantum

Received October 2, 2014; in final form April 14, 2015.
*Corresponding author. E-mail: andris.anspoks@cfi.lu.lv
Color versions of one or more figures in this article can be found online at www.tandfonline.com/gfer.

paraelectricity [5, 6, 7]). This leads to the idea that ferroelectricity in STO can be induced by suppression of the quantum fluctuations. Experimentally, this was observed using isotope exchange (^{16}O with ^{18}O) [8].

There is long debate about structure of polar phase and mechanism of the phase transition in $SrTi^{18}O_3$. The first mechanism proposed was the displacive type, caused by the condensation of the ferroelectric E_u soft mode [9, 10, 11, 12], the second was the addition of an order-disorder type component to the displacive soft mode one [13, 14, 15, 16].

The structure of STO has been studied by different experiments: X-ray diffraction (XRD) [17, 18], neutron diffraction [19, 20] and X-ray absorption spectroscopy [21, 22, 23, 24, 25, 26, 27, 28] but clear picture and consistence of opinions have not been achieved still.

In this work the local atomic structure around Ti in $SrTi^{16}O_3$ and $SrTi^{18}O_3$ is studied in the temperature range 8 – 300 K with X-ray absorption spectroscopy methods, namely extended x-ray absorption fine structure (EXAFS), advanced reverse Monte Carlo (RMC) and evolutionary algorithm (EA) techniques for EXAFS data analysis (RMC/EA-EAXFS) [29].

Experimental

In our study we used two powder samples: standard $SrTi^{16}O_3$ (STO16) with 100% ^{16}O (STO16) and $SrTi^{18}O_3$ (STO18) where 96 % of ^{16}O atoms were substituted by ^{18}O isotope. STO18 sample crystals preparation procedure has been previously described in ref. [9].

The Ti K-edge x-ray absorption spectra were measured in transmission mode at the ESRF bending-magnet beamline BM23 and at the HASYLAB/DESY A1 bending-magnet beamline in the temperature range 8 K – 300 K. The x-ray radiation was monochromatized by a 40 % detuned Si(111) double-crystal monochromator, and the beam intensity was measured using two ionization chambers filled with argon and krypton gases. The temperature of the sample was stabilized on $\pm$ 0.1 K with He flow cryostat. To achieve the best sample homogeneity and thickness at the Ti K-edge, necessary for transmission mode experiments, the proper amount of the STO powder was deposited on polytetraflouroethylene Millipore membranes from suspensions in methyl alcohol.

The Extended X-ray absorption fine structure (EXAFS) oscillations data χ(k) were extracted following the conventional procedure [30, 31] using the EDA software package [32].

The extracted STO16 EXAFS spectra $\chi(k)k^2$ and corresponding Fourier transforms are shown in Fig. 1. Spectra of STO18 and STO16 look very similar, as it was expected since difference in the structure between STO18 and STO16 is very small [8]. The peak of the first coordination shell (is seen in Fourier transform between 1 and 2 Å) contains only the single scattering signals. The peaks located between 2.5 and 4 Å correspond to the second (Sr atoms) and the third (Ti atoms) coordination shell of Ti, which are very close and cannot be separated; moreover they contain multiple scattering contributions from different Ti-O-Ti chains and triangles. At the same time, one can see that that Ti-Sr contribution is very sensitive towards temperature, unlike the ones from Ti-Ti and Ti-O.

RMC/EA-EXAFS Simulations

The best method to analyze these data is reverse Monte Carlo (RMC) and evolutionary algorithm (EA) techniques for EXAFS data analysis (RMC/EA-EAXFS) [29]. The

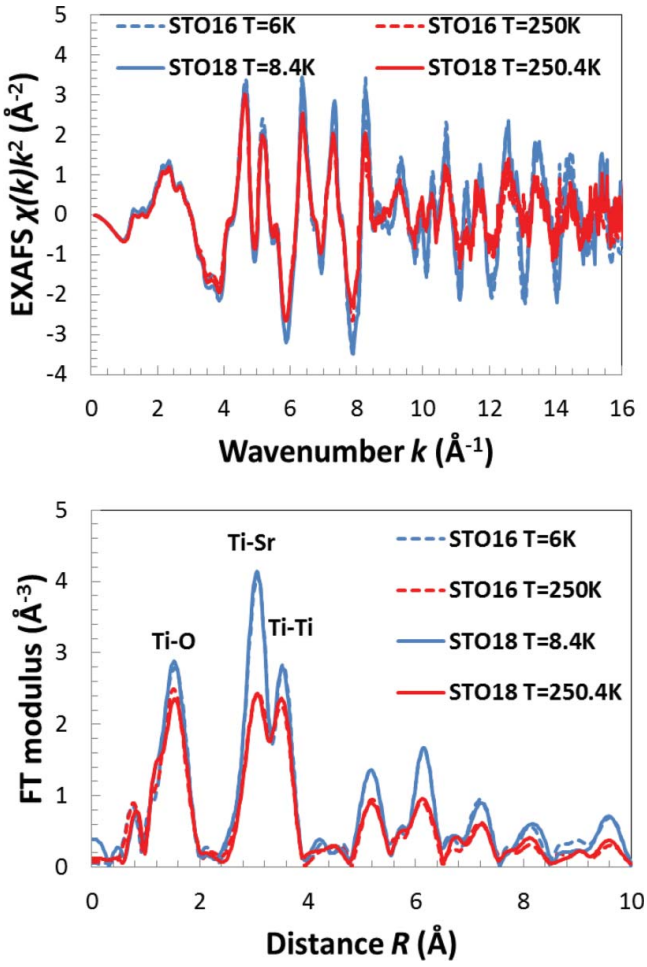

Figure 1. Ti K-edge EXAFS spectra for STO16 and STO18 at selected temperatures and their Fourier transform (FT). Note that the positions of the FT peaks are shifted from their true crystallographic values because the FTs were calculated without phase-shift corrections.

method does not restrict the geometry of the system (in our case no limitations to the distortions of the oxygen octahedra and positions of Ti and Sr atoms in it) and takes into account all multiple scattering effects, which are very sensitive to the bonding angles and distances, e.g. in Ti-O-Ti chains and triangles.

In RMC/EA-EXAFS simulations we used 32 supercells, where each supercell with size $4a \times 4b \times 4c$ contains 1280 atoms. Lattice constants *a, b* and *c* were taken from diffraction studies [20].

Comparison of the experimental and theoretical EXAFS spectra has been performed using a Morlet wavelet transform (WT) [33, 34] in 3 Å^{-1} – 16 Å^{-1} of the *k*-space, and 0.9 Å – 4.5 Å of the *R*-space range.

Being a straightforward mathematical procedure as the Fourier transform, the WT allows one to obtain a two-dimensional representation of the periodic signal with simultaneous localization in *k* and *R* spaces that is an advantage over conventional fit in *k* or *R*

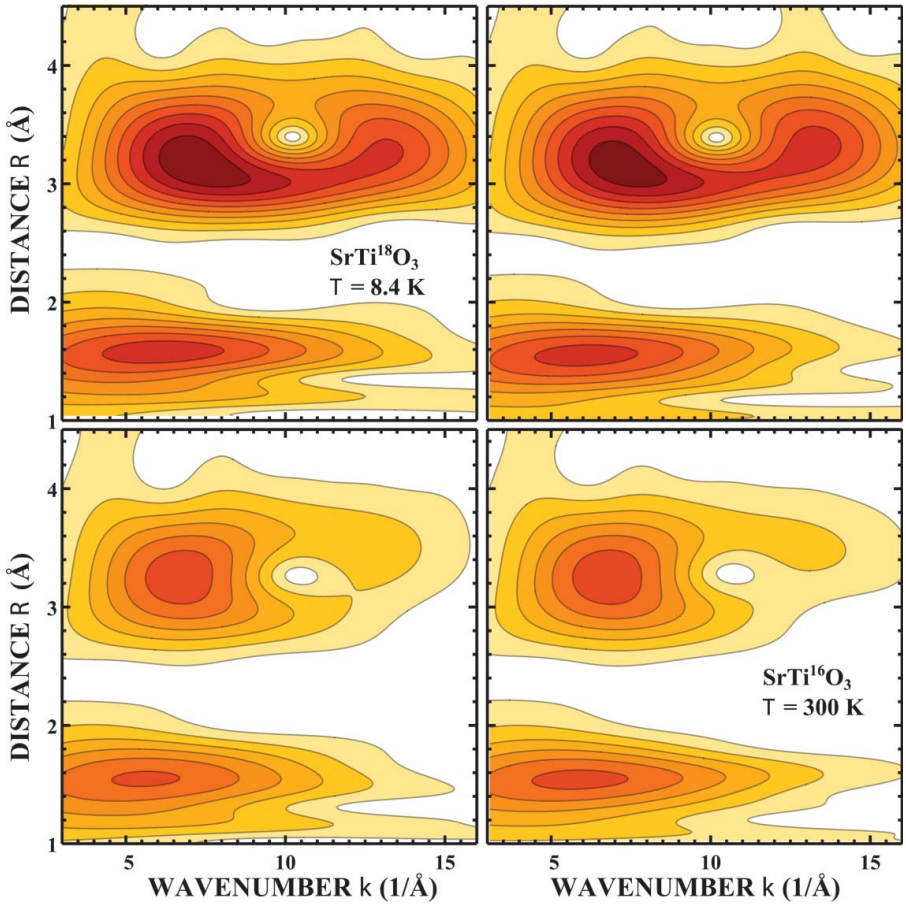

Figure 2. Wavelet analysis of Ti K-edge EXAFS data for STO16 and STO18 at selected temperatures, performed using Morlet wavelet transform.

space only. In the case of STO for instance, WT allows one to discriminate contributions from Ti-Ti and Ti-Sr atom pairs. From Fig. 2, one can directly see, for example, that Ti-Sr contribution, unlike the one from Ti-Ti and Ti-O, is very sensitive towards temperature. Also differences between STO18 and STO16 spectra can be better noticed using the WT method then the standard EXAFS analysis methods (Fig. 2.).

Usage of WT for data fitting in our case has also the advantage that it allows to better separate the contribution to the total EXAFS of the first coordination shell (Ti-O) from the noise due to imperfections in background subtraction procedure.

Scattering paths with the half-path length up to 5.5 Å and the multiple-scattering contributions up to the third order were considered in our simulations. The calculation of the cluster potential was performed only once for the average atom configuration, corresponding to the $SrTiO_3$ crystallographic structure. The complex exchange-correlation Hedin-Lundqvist potential and default values of muffin-tin radii, as provided within the FEFF8 code [35], were employed. As the output of RMC/EA-EXAFS analysis we have obtained a set of atomic coordinates, which can be used to calculate radial distribution functions, average distance between atoms, MSRD, and other values.

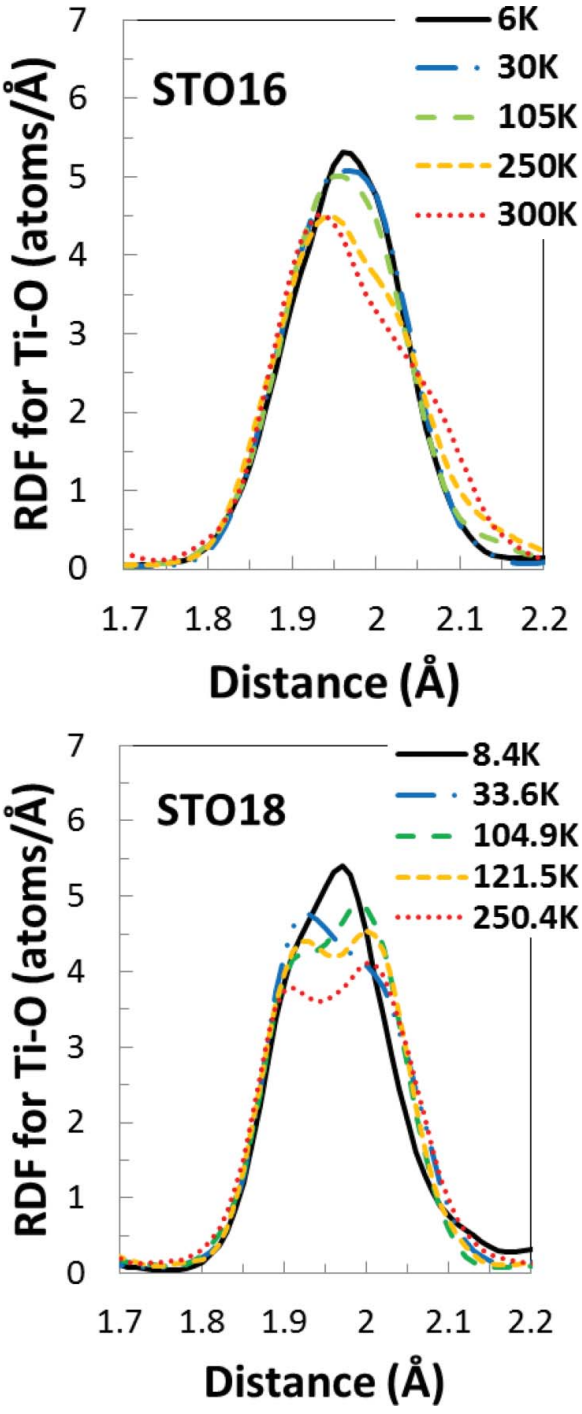

Figure 3. RDF for the first coordination shell of Ti (Ti-O).

Results and Discussion

The obtained shapes for Ti-O radial distribution function (RDF) are shown in Fig. 3, where two distinct groups of the oxygen atoms separated by about 0.1 Å are recognizable in the first coordination shell of Ti for STO18 in the whole range of temperatures.

At the same time, the RDF for STO16 contains less pronounced features: the non-Gaussian shape of the Ti-O RDF remains in the whole range of the temperatures.

Evidence of similar distortions was previously documented for STO by Fisher et al. [21] and for $BaTiO_3$ by Ravel et al. [36].

On the contrary, the presence of a single dominating distance between Ti-Ti is evident in Fig. 4: this is a sign of strong correlation between neighboring Ti atoms.

The RDF corresponding to the distribution of Ti-Sr distances shows strong temperature dependence (Fig. 5). The shape of the RDF does not change significantly; all features only flatten with the increase of the temperature, indicating increasing thermal disorder.

The mean-square relative displacement (MSRD) values are shown in Figs. 6 and 7. MSRDs are calculated as the second moment of the RDF. At the first glimpse one can see that all values do not follow classical Einstein-like temperature behavior, especially for STO18.

It is seen that the absolute values of Ti-O MSRD in the low temperature region for STO18 are larger than those for STO16. This confirms our previous studies using X-ray absorption near edge structure studies [37]. This is mainly due to the presence of the displacements of Ti atoms from the central position, as already documented by Ti-O RDF (Fig. 3).

Ti-O MSRD for STO18 shows a quite well distinguishable peak around 25 K, where transition to polar phase occurs. This can be a sign of fluctuations, leading to larger dynamic and/or static displacements of Ti in the oxygen octahedra.

Ti-Ti MSRD temperature dependence for STO18 and STO16 (Fig. 6) is nearly flat till 110K. Above AFD PT point it slightly increases and again remains nearly constant at least in the temperature range 150 – 250 K.

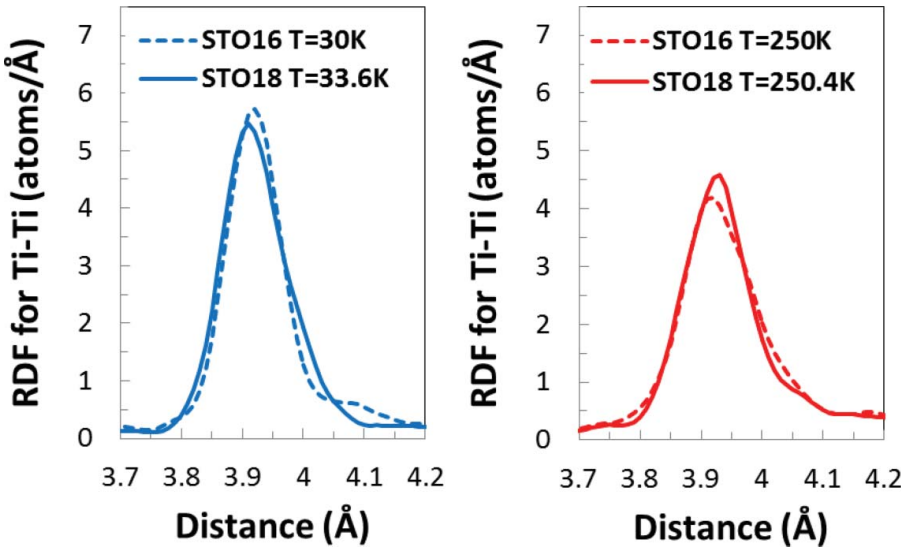

Figure 4. RDF for the third coordination shell of Ti (Ti-Ti).

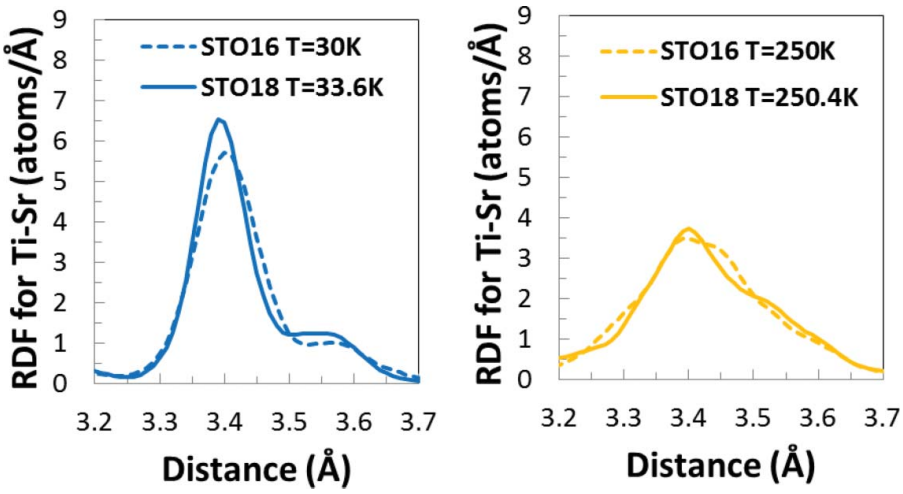

Figure 5. RDF for the second coordination shell of Ti (Ti-Sr).

Ti-Sr MSRD shows Einstein-like temperature behavior in the high temperature region corresponding to the cubic phase.

Ti-Sr MSRD for STO18 shows jump-like discontinuity at 25 K. Increased values at polar phase may be correlated with the observed increased static disorder for Ti. No anomalies are observed for Ti-Sr MSRD for STO16 in the low temperature region.

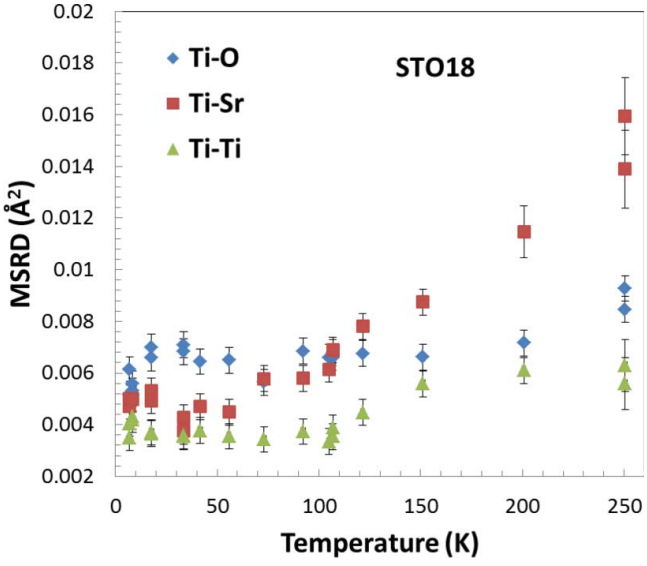

Figure 6. MSRD values for first three coordination shells of Ti for STO18.

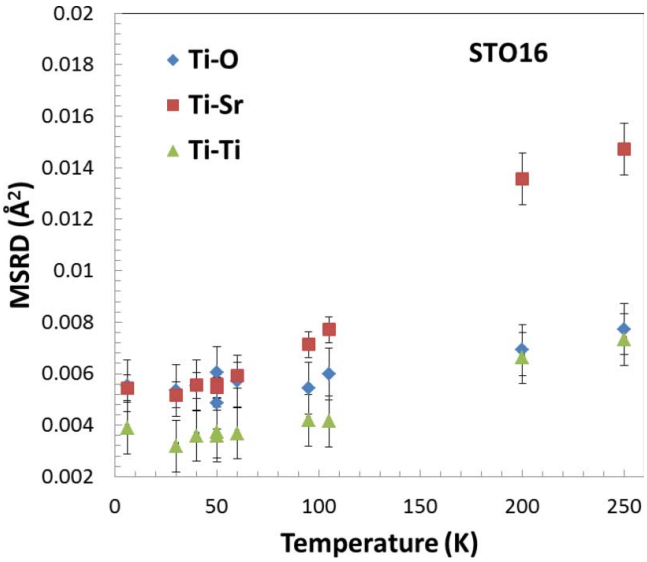

Figure 7. MSRD values for first three coordination shells of Ti for STO16.

Conclusions

Obtained results show non-Gaussian character of the RDF for the first three coordination shells of Ti, especially the first shell in the whole temperature range studied (8 – 300 K).

We have found that there are well resolved two groups of oxygen atoms (separated by ~ 0.1Å) in the Ti-O RDF in the first coordination shell of Ti in STO18, which remain in the whole range of the temperatures (from 8 to 300 K).

The same applies to STO16, but the corresponding distance between two groups of oxygen atoms is smaller.

The absolute values for the first coordination shell of Ti (Ti-O) MSRD in the low temperature region for STO18 are larger than those for STO16.

The MSRD values for the first coordination shell of Ti in STO18 have noticeable anomaly in the vicinity of the low-T phase transition into polar phase (25 K).

At the same time, there is a strong correlation between nearest neighboring Ti atoms (corresponding to the third coordination shell of Ti) for STO18 in the whole range of the temperatures (8 – 300 K), as it is seen in the shape of RDF and further supported by the constant MSRD value for STO18 Ti-Ti distances in between 8 – 106 K, and nearly constant value in the 150–250 K region. Ti-Ti MSRD values show noticeable anomaly around AFD PT in the 105 – 150 K region.

MSRD for Ti-Sr have the strongest temperature dependence with the Einstein-like temperature behavior in the high temperature region corresponding to the cubic phase. Ti-Sr MSRD for STO18 shows jump-like discontinuity at 25 K which may be correlated with the observed increased static disorder for Ti. No anomalies are observed for Ti-Sr MSRD for STO16 in the low temperature region.

The nature of these effects observed can be static or dynamic. These two effects cannot be separated by EXAFS data analysis since the small averaging time (10^{-15} s) of XAS technique [38].

It is important that our measurements revealed presence of some static and dynamic disorders in STO16, more pronounced in STO-18. It can be connected to precursor effect widely discussed today and to results by Golovenchits et al. [39]. It was suggested that a strongly frustrated state in STO at low temperatures is realized due to an interaction between the structural and ferroelectric order parameters. Such low temperature state of STO was treated as *a* critical one near the paraelectric-ferroelectric phase transition. In such scenario pronunciation of polar ordering precursor effects in STO-18 in comparison with STO-16 looks quite natural.

Acknowledgments

The authors thank Dr. Olivier Mathon from ESRF and Dr. Edmund Welter from DESY for assistance during the beamtimes, and Dr. Alexei Kuzmin for fruitful discussions and feedback.

Funding

This work has been supported by the Latvian Science Council grant no. 402/2012. The work was supported in part from large infrastructure SAFMAT Project CZ.2.13/3.1.00/22132, P108/12/1941 of GACR and PP RAS "Quantum mesoscopic and disordered systems".

References

1. M. E. Lines, and A. M. Glass, Principles and Applications of Ferroelectrics and Related Materials (Oxford: Clsarendon Press) p 680 (1977).
2. P. A. Fleury, J. F. Scott, and J. M. Worlock, SOFT PHONON MODES AND THE 110'K PHASE TRANSITION IN $SrTiO_3$. *Phys. Rev. Lett.* **21**, 16–19 (1968).
3. G. Shirane, and Y. Yamada, Lattice-Dynamical Study of the 110 K Phase Transition in $SrTiO_3$. *Phys. Rev.* **177**, 858–863 (1969).
4. J. H. Barrett, Dielectric Constant in Perovskite Type Crystals. *Phys. Rev.* **86**, 118–120 (1952).
5. K. A. Muller, and H. Burkard, $SrTiO_3$: An intrinsic quantum paraelectric below 4 K. *Phys. Rev. B* **19**, 3593–3602 (1979).
6. V. G. Vaks, Introduction to Microscopical Theory of Ferroelectrics Moscow: Nauka p 327 (in Russian) 1973.
7. O. E. Kvyatkovskii, Quantum Effects in Incipient and Low-Temperature Ferroelectrics (A Review). *Phys. Sol. State* **43** 1345–1362 (2001).
8. M. Itoh, R. Wang, Y. Inaguma, T. Yamaguchi, Y. J. Shan, and T. Nakamura, Ferroelectricity Induced by Oxygen Isotope Exchange in Strontium Titanate Perovskite. *Phys. Rev. Lett.* **82**, 3540–3543 (1999).
9. H. Taniguchi, M. Itoh, and T. Yagi, Ideal Soft Mode-Type Quantum Phase Transition and Phase Coexistence at Quantum Critical Point in ^{18}O-Exchanged $SrTiO_3$. *Phys. Rev. Lett.* **99**, 017602 (2007).
10. H. Hasebe, Y. Tsujimi, R. Wang, M. Itoh, and T. Yagi, Dynamical mechanism of the ferroelectric phase transition of $SrTi^{18}O_3$ studied by light scattering. *Phys. Rev. B* **68**, 014109 (2003).
11. M. Takesada, M. Itoh, and T. Yagi, Perfect Softening of the Ferroelectric Mode in the Isotope-Exchanged Strontium Titanate. *Phys. Rev. Lett.* **96**, 227602 (2006).
12. H-Y Deng, C-H Lam, H. T. Huang, On the origin of oxygen isotope exchange induced ferroelectricity in strontium titanate. *Eur. Phys. J. B* **85**, 234 (2012).

13. R. Blinc, B. Zalar, V. V. Laguta, M. Itoh, Order-Disorder Component in the Phase Transition Mechanism of ^{18}O Enriched Strontium Titanate. *Phys. Rev. Lett.* **94**, 147601 (2005).
14. T. Shigenari, K. Abe, T. Takemoto, O. Sanaka, T. Akaike, Y. Sakai, R. Wang, and M. Itoh, Raman spectra of the ferroelectric phase of $SrTi^{18}O_3$: Symmetry and domains below Tc and the origin of the phase transition. *Phys. Rev. B* **74**, 174121 (2006).
15. A. Bussmann-Holder, and A. R. Bishop, Incomplete ferroelectricity in $SrTi^{18}O_3$. *Eur. Phys. J. B* **53**, 279–282 (2006).
16. J. F. Scott, J. Bryson, M. A. Carpenter, J. Herrero-Albillos, and M. Itoh, Elastic and Anelastic Properties of Ferroelectric $SrTi^{18}O_3$ in the kHz-MHz Regime. *Phys. Rev. Lett.* **106**, 105502 (2011).
17. F. W. Lytle, X-Ray Diffractometry of Low Temperature Phase Transformations in Strontium Titanate. *J. Appl. Phys.* **35**, 2212–2215 (1964).
18. M. Schmidbauer, A. Kwasniewski, and J. Schwarzkopf, High-precision absolute lattice parameter determination of $SrTiO_3$, $DyScO_3$ and $NdGaO_3$ single crystals. *Acta Cryst. B* **68**, 8–14 (2012).
19. A. Heidemann, and H. Wettengel, Die Messung der Gitterparameter/inderung von $SrTiO_3$. *Z. Phys.* **258**, 429–438 (1973).
20. Q. Hui, M. G. Tucker, M. T. Dove, S. A. Wells, D. A. Keen, Total scattering and reverse Monte Carlo study of the 105 K displacive phase transition in strontium titanate. *J. Phys.: Condens. Matter* **17**, S111–S124 (2005).
21. M. Fischer, A. Lahmar, M. Maglione, A. San Miguel, J. P. Itie, and A. Polian, Local disorder studied in $SrTiO_3$ at low temperature by EXAFS spectroscopy. *Phys. Rev. B* **49**, 12451–12456 (1994).
22. B. Ravel, and E. A. Stern, Local disorder and near edge structure in titanate perovskites. *Physica B* **208/209**, 316–318 (1995).
23. O. Kamishima, Y. Nishihata, H. Maeda, T. Ishii, A. Sawada, and H. Terauchi, EXAFS study on the local structure in strontium titanate. Physica B **208/209**, 303–304 (1995).
24. S. Nozawa, T. Iwazumi, and H. Osawa, Direct observation of the quantum fluctuation controlled by ultraviolet irradiation in $SrTiO_3$. *Phys. Rev. B* **72**, 121101 (2005).
25. B. P. Andreasson, M. Janousch, U. Staub, G. I. Meijer, B. Delley, Resistive switching in Cr-doped $SrTiO_3$: An X-ray absorption spectroscopy study. Mat. Sci. Eng. B **144**, 60–63 (2007).
26. T. Hashimoto, A. Yoshiasa, M. Okube, H. Okudera, and A. Nakatsuka, Temperature dependence of XANES spectra for $ATiO_3$, A_2TiO_4 and TiO_2 compounds with structural phase transitions. *AIP Conf. Proc.* **882**, 428–430 (2007).
27. M. Vračar, A. Kuzmin, R. Merkle, J. Purans, E. A. Kotomin, J. Maier, and O. Mathon, Jahn-Teller distortion around Fe^{4+} in $Sr(Fe_xTi_{1-x})O_{3-\delta}$ from x-ray absorption spectroscopy, x-ray diffraction, and vibrational spectroscopy. *Phys. Rev. B* **76**, 174107 (2007).
28. I. Levin, V. Krayzman, J. C. Woicik, A. Tkach, and P. M. Vilarinho, X-ray absorption fine structure studies of Mn coordination in doped perovskite $SrTiO_3$. *Appl. Phys. Lett.* **96**, 052904 (2010).
29. J. Timoshenko, A. Kuzmin, J. Purans, EXAFS study of hydrogen intercalation into ReO_3 using the evolutionary algorithm. *J. Phys.: Condens. Matter* **26**, 055401 (2014).
30. J. J. Rehr, and R. C. Albers, Theoretical approaches to x-ray absorption fine structure. *Rev. Mod. Phys.* **72**, 621–654 (2000).
31. V. L. Aksenov, M. V. Kovalchuk, A. Kuzmin, J. Purans, S. I. Tyutyunnikov, Development of methods of EXAFS spectroscopy on synchrotron radiation beams. *Crystallogr. Rep.* **51**, 908–935 (2006).
32. A. Kuzmin, EDA: EXAFS data analysis software package. *Physica B* **208–209**, 175–176 (1995).
33. M. Munoz, P. Argoul, F. Farges, Continuous Cauchy wavelet transform analyses of EXAFS spectra: a qualitative approach. *Am. Mineral.* **88**, 694–700 (2003).
34. J. Timoshenko, A. Kuzmin, Wavelet data analysis of EXAFS spectra. *Comp. Phys. Commun.* **180**, 920–925 (2009).

35. A. L. Ankudinov, B. Ravel, J. J. Rehr, and S. D. Conradson, Real-space multiple-scattering calculation and interpretation of x-ray-absorption near-edge structure. *Phys. Rev. B* **58**, 7565–7576 (1998).
36. B. Ravel, E. A. Stern, R. I. Vedrinskii, and V. Kraizman, Local Structure and the Phase Transition of $BaTiO_3$. *Ferroelectric* **206**, 407–430 (1998).
37. A. Anspoks, D. Bocharov, J. Purans, F. Rocca, A. Sarakovskis, V. Trepakov, A. Dejneka, M. Itoh, Local structure studies of $SrTi^{16}O_3$ and $SrTi^{18}O_3$. *Phys. Scripta* **89**, 044002 (2014).
38. E. A. Stern, Character of Order-Disorder and Displacive Components in Barium Titanate. *Phys. Rev. Lett.* **93**, 037601 (2004).
39. E. Golovenchits, V. Sanina, and A. Babinsky, Nonlinear dielectric susceptibility and the possible origin of the low temperature state of $SrTiO_3$. Ferroelectrics **199**, 317–325 (1997).